LETTER

Probing the electromagnetic field of a 15–nanometre hotspot by single molecule imaging

Hu Cang[1,2], Anna Labno[2,3], Changgui Lu[2], Xiaobo Yin[1,2], Ming Liu[2], Christopher Gladden[2], Yongmin Liu[2] & Xiang Zhang[1,2]

When light illuminates a rough metallic surface, hotspots can appear, where the light is concentrated on the nanometre scale, producing an intense electromagnetic field. This phenomenon, called the surface enhancement effect[1,2], has a broad range of potential applications, such as the detection of weak chemical signals. Hotspots are believed to be associated with localized electromagnetic modes[3,4], caused by the randomness of the surface texture. Probing the electromagnetic field of the hotspots would offer much insight towards uncovering the mechanism generating the enhancement; however, it requires a spatial resolution of 1–2 nm, which has been a long-standing challenge in optics. The resolution of an optical microscope is limited to about half the wavelength of the incident light, approximately 200–300 nm. Although current state-of-the-art techniques, including near-field scanning optical microscopy[5], electron energy-loss spectroscopy[6], cathode luminescence imaging[7] and two-photon photoemission imaging[8] have subwavelength resolution, they either introduce a non-negligible amount of perturbation, complicating interpretation of the data, or operate only in a vacuum. As a result, after more than 30 years since the discovery of the surface enhancement effect[9–11], how the local field is distributed remains unknown. Here we present a technique that uses Brownian motion of single molecules to probe the local field. It enables two-dimensional imaging of the fluorescence enhancement profile of single hotspots on the surfaces of aluminium thin films and silver nanoparticle clusters, with accuracy down to 1.2 nm. Strong fluorescence enhancements, up to 54 and 136 times respectively, are observed in those two systems. This strong enhancement indicates that the local field, which decays exponentially from the peak of a hotspot, dominates the fluorescence enhancement profile.

The study of the surface enhancement effect mirrors the development of surface analysis techniques. Previous optical experiments revealed that the roughness of the surface has a critical role in determining the strength of the enhancement[9,11]. Further experimental[12] and theoretical[13] studies on the impact of the surface roughness led to the connection between the surface enhancement effect and the surface plasmon, as well as to the hotspots being termed localized surface plasmon polaritons[4,13–15]. More recently, near-field scanning optical microscopy[16], electron energy-loss spectroscopy[6], cathodoluminescence imaging[7], two-photon photoemission imaging[8] and experiments with a waveguide mode excitation[17] have shown that, at these hotspots, the fluorescence enhancement is confined to a region far smaller than the wavelength of light, yet the field of a single hotspot has not been resolved.

We developed a single molecule super-resolution imaging method, based on the fact that individual fluorescent molecules can be localized with single-nanometre accuracy from the optical far field. When multiple emitters reside within a diffraction-limited spot, one has to ensure that these emitters emit one at a time[18–21]. Control of the emitting sequence can be done by serial photo-switching of fluorescence molecules[18,19], using techniques such as photo-activated localization microscopy[18] and stochastic optical reconstruction microscopy[19]. These

techniques, together with structural illumination microscopy and stimulated emission depletion microscopy, allow optical resolution beyond the diffraction limit in biological samples (for a review, see ref. 22). As photo-switching would be infeasible for investigating local field, we use the Brownian motion of single dye molecules[20,21,23] in a solution to let the dyes scan the surface of single hotspots in a stochastic manner, one molecule at a time.

Figure 1a illustrates the principle of this new technique. Here, a sample is submerged in a solution of fluorescent dye. The chamber containing the sample is mounted on a total internal reflection (TIRF) set-up. As the diffusion of the dye molecules is much faster than the image acquisition time (a 1-nm-diameter sphere diffuses through a 200-nm-wide spot in less than 0.1 ms on average in water at room temperature, in contrast to an imaging time of typically 50–100 ms), the fluorescence from the rapidly diffusing dye molecules contributes only to a homogeneous background. When a dye molecule is adsorbed onto the surface of a hotspot, it appears as a bright spot. By using a maximum likelihood single molecule localization method[24] (Supplementary Information), the molecule can be localized with single-nanometre accuracy[18–21], and the fluorescence enhancement can be deduced from the intensity of the fluorescence. After the dye molecule is bleached, which typically occurs within hundreds of milliseconds, the fluorescence disappears and the hotspot is ready for the next adsorption event. By choosing the right concentration of dye molecules, the adsorption rate can be controlled to the point of ensuring that only one molecule emits at a time. As we use a camera to record single molecule adsorption events, multiple hotspots within a large field of view of up to 1 mm^2 can be imaged in parallel. This is much more efficient than raster scanning based techniques, such as near-field scanning optical microscopy and electron energy-loss spectroscopy.

Using this method, we are able to image the fluorescence enhancement profile of single hotspots as small as 15 nm with an accuracy down to 1.2 nm, well beyond the diffraction limit, in just a few minutes (Supplementary Movie; Fig. 1b). The hotspots are formed on the surface of a thin (12–15 nm) aluminium film deposited on a quartz substrate by electron-beam evaporation. Water facilitates the oxidization process[25]; an oxidized layer can form on the surface of the aluminium film and reach a thickness of up to 8 nm (ref. 25). Each sphere in Fig. 1b represents a single molecule adsorption event, with the x and y coordinates representing the location of the molecule's centroid, and the z coordinate corresponding to the intensity of the molecule's fluorescence. Single molecules can be localized with an accuracy down to 1.2 nm (Fig. 1c; Supplementary Information). The measured enhancement here exhibits a rapid exponential decay with a decay constant of 9.8 nm (Fig. 1d, e). The standard deviation of the location of observed single molecule events was used as a model-independent measure of the width (15.4 nm) of the hotspot, as shown in Fig. 1f. The existence of such a small hotspot demonstrates the presence of tight near-field optical confinement.

The accurate estimation of the hotspot enhancement and electromagnetic field experienced by the molecule is confounded by a number

---

[1]Materials Sciences Division, Lawrence Berkeley National Laboratory, Berkeley, California 94720, USA. [2]NSF Nano Scale Science and Engineering Center (NSEC), 3112 Etcheverry Hall, University of California, Berkeley, California 94720, USA. [3]Biophysics Program, University of California Berkeley, Berkeley, California 94720, USA.
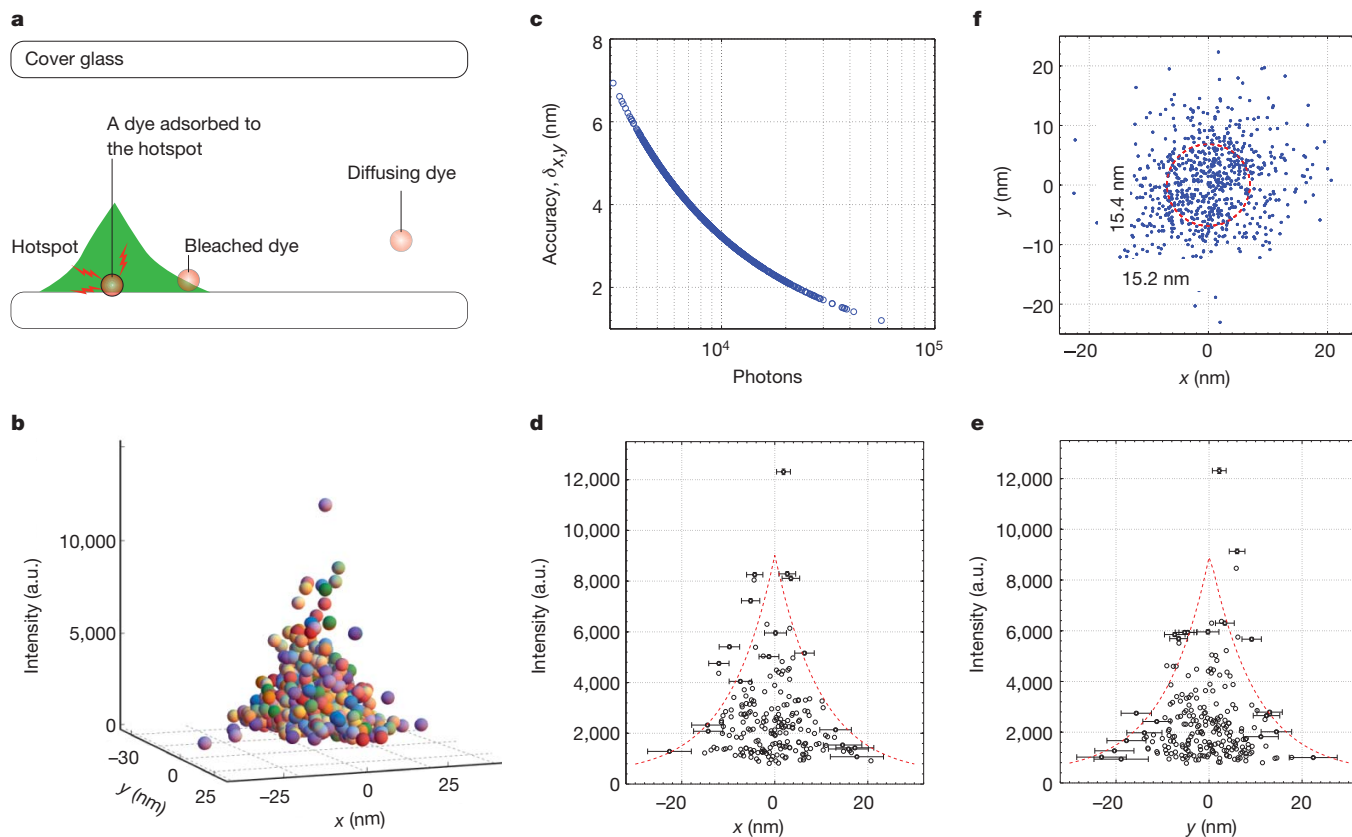
Figure 1 | The principle of Brownian motion single molecule super-resolution imaging. a, Hotspots appear on the surface of a thin aluminium film under a total internal reflection (TIRF)-type illumination at 532 nm. To map the field distribution inside the hotspots, we use the Brownian motion of fluorescence dye molecules (Chromeo 546). The dye molecules stochastically adsorb to the surface. After a few frames (50–100 ms per frame), the dye molecules photobleach, give rise to a 'blinking' pattern (Supplementary Movie): each blink corresponds to one adsorption-bleaching event. By controlling the concentration of the dyes, the adsorption rate can be adjusted to ensure that within a diffraction limited spot, only one molecule emits photons at a time; therefore the position of the molecule can be determined by a maximum likelihood localization method[24] with accuracy down to 1.2 nm (**c**). **b**, By using the adsorption locations as the x and y coordinates, and the fluorescence intensity as the z coordinate, we obtain a 3D scatter plot of the fluorescence enhancement profile of the hotspot, with each sphere representing one single molecule event. **c**, The accuracy of the reconstructed field profile, estimated from the variance of the maximum likelihood localization[24] (Supplementary Information), depends on the number of photons collected from the molecules, with brighter single molecule events showing better accuracy, down to 1.2 nm. The molecules within $-2\,\text{nm} < y < 2\,\text{nm}$ are shown in **d**, which represents a cross-section of the hotspot at $y = 0$ nm. A similar plot of the cross-section of the hotspot at $x = 0$ nm is shown in **e**. The envelope appears as an exponential decay with a constant of 9.83 nm (red dashed lines). To avoid crowding, only the single molecule localization variance of a few spheres near the envelope is shown. **f**, The distribution of the single molecule events provides a direct measure of the size of the hotspot; the width of the hotspot characterized by the standard deviation of the single molecule events is 15.2 nm and 15.4 nm in x and y directions, respectively.

of factors, including the molecule's orientation relative to the polarization of local field, and stochastic photobleaching (Supplementary Information). To decrease the effect of those stochastic variables on the final shape of the profile, we use a Gaussian kernel method to render the image of a hotspot[18], as shown in Fig. 2a. Each pixel X of the rendered image, $I(X)$, is a weighted average of the intensity from all of the single molecule events, with molecules closer to X carrying more weight (Fig. 2a). The window size of the kernel is determined by the accuracy of the single molecule localization. The rendered image reports an averaged profile of the local fluorescence enhancement. A hotspot may have complex structures that are smaller than the size of the kernel; these fine structures are removed in the stochastic rendering process (Supplementary Information). The exponential decay is evident, with the full-width at half-maximum (FWHM) measured as ~20 nm (Fig. 2b).

By comparing the fluorescence from the dye molecules adsorbed on the hotspot to that from the dye molecules immobilized on the surface of a quartz slide under the same conditions (Supplementary Information), we determined that the fluorescence enhancement is about 36 times greater at the centre of the 20-nm hotspot. This modest enhancement results from the high ohmic loss of aluminium at the visible wavelength involved. Among the total of 60 hotspots that were analysed, we found a broad distribution of enhancement factors and sizes,

with approximately 32 nm as the average size of the spots (Fig. 2c). The maximum fluorescence enhancement factor of the hotspots was found to depend inversely on their size; the largest enhancement factor we observed was 54 times (for a 15-nm hotspot); this results from the tighter confinement of the electromagnetic field in a smaller hotspot (Fig. 2d).

As hotspots also appear in metal nanoparticle clusters[12,13], and the mechanism has been postulated to be similar to that of the metal thin films, we investigated the hotspots that formed in silver clusters consisting of silver nanoparticles with average diameter of 40 nm. In addition to the oxidation layer of silver[26], the dispersing surfactant (that comes with the silver nanoparticle suspension) condenses on the surface of the silver nanoparticle clusters during the aggregation process. We found that the fluorescence enhancement profile of the hotspots formed in the silver clusters has an exponential shape, similar to that of hotspots on the surface of an aluminium film (Fig. 3a, b). The electromagnetic field is strongly confined in a hotspot within an elliptical region of 13.2 nm × 20.3 nm, more than 30 times smaller than the wavelength of the excitation laser (Fig. 3c).

The fluorescence enhancement includes contributions from both local field and quenching. Experiments have shown that the quenching—transfer of energy from molecules to the metal nanostructure[27]—is
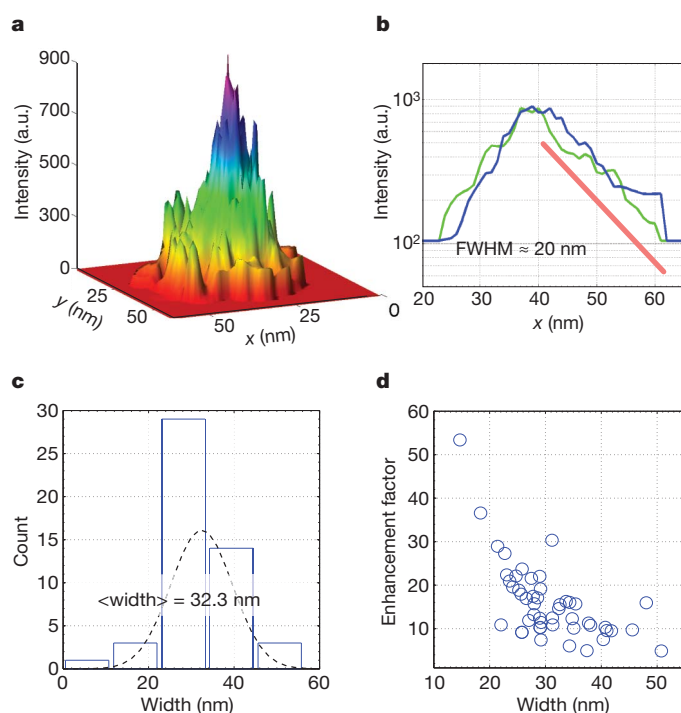
Figure 2 | Hotspots on an aluminium film. a, As the fluorescence of a single molecule is intrinsically stochastic, we remove this randomness by using a Gaussian kernel method to render the image of the field distribution. A hotspot on the surface of an aluminium film is shown. Each pixel X of the rendered image corresponds to average intensity from all of the single molecule events, with molecules closer to X carrying more weight. The kernel window size is 2.1 nm; this small window size makes the image appear noisy. An exponential decay field profile is visible, and is more evident on a log scale, shown in **b** as almost a decade of straight line (red solid line). The blue and green curves are two cross-sections of the hotspot along x and y directions through the peak. The FWHM of the spot is ∼20 nm. **c**, All of the hotspots observed are of deep sub-wavelength size, with an average width of 32.3 nm. By plotting the enhancement factor of the hotspots against their width (**d**), an inverse relationship between the size and the enhancement factor is visible: tighter confinement leads to stronger enhancement.

short-ranged compared to the local field. Therefore there exist two distinct regimes above the surface of a metal: a quenching dominated regime near the surface, followed by a local field dominated regime further away from the surface[26,28]; the transition point between the two regimes coincides with the peak of the fluorescence enhancement. This peak ranges from a few nanometres to tens of nanometres, depending on the materials and the geometry of the nanostructures[26,28]. The dielectric layers formed on the surface of the metal shift the adsorbed layer of molecules into the local field dominant regime, contributing to the strong (up to 54 times (Al) and 136 times (Ag)) fluorescence enhancement observed. To reproduce the effect of the dielectric layers, we deposited a ∼9-nm-thick spacer layer of self-assembled protein molecules on the surface of silver nanoparticle clusters *in situ*, in addition to the original dielectric layer (Supplementary Information). As the transition point of silver nanoparticle clusters is ∼2.5 nm above the surface in a similar system[26], the observation will be in the local field dominant regime. Comparing the same hotspot without and with the spacer layer, we found an ∼36% drop in the fluorescence enhancement, an ∼26% increase in width, and an essentially unchanged exponential shape (Supplementary Information), which confirms that an exponential profile is a general feature of the local electromagnetic field.

The single molecule super-resolution approach is a generic technique, which offers a unique, perturbation free capability for imaging the electromagnetic field enhancement of optical nanostructures with single-nanometre precision. Using this technique, we have
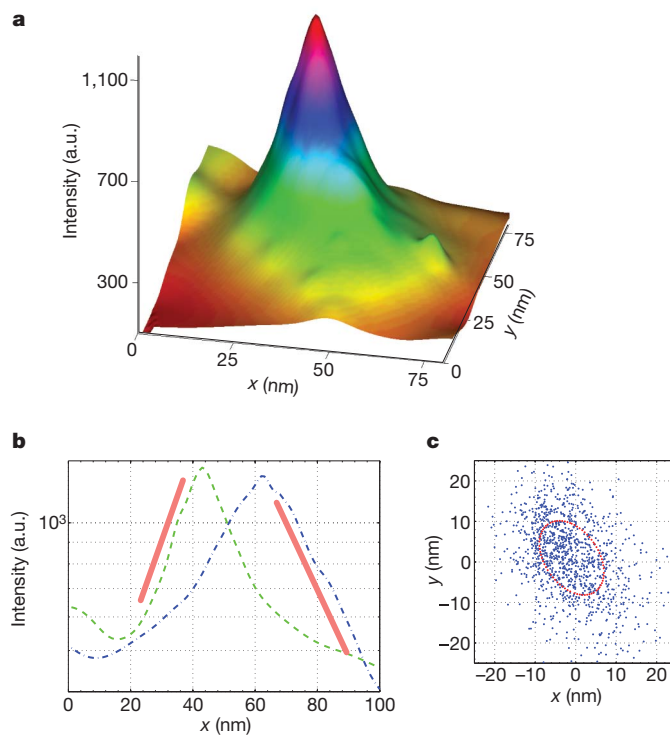
Figure 3 | A hotspot on silver nanoparticle clusters. a, A hotspot formed on silver nanoparticle clusters appears similar to those formed on the aluminium film. A 644-nm laser is used for excitation, and Chromeo 642 dye (Active Motif)—whose emission centres around 660 nm—is used. The maximum enhancement factor at the centre of the peak corresponds to 136 times the florescence from the same dye molecules adsorbed on a glass surface. **b**, The hotspot exhibits a similar exponential decay profile as those formed on the surface of the aluminium film. Two cross-sections of the hotspot along x (green) and y (blue) directions through the peak are plotted on a logarithmic scale, with the solid red lines as eye-guides for the exponential profile. **c**, The widths of the hotspot, estimated from the distribution of the single molecule events on a scatter plot, are 13.2 nm and 20.3 nm along the two axes.

demonstrated the first (to our knowledge) direct measurement of a single hotspot as small as 15 nm and with an accuracy down to 1.2 nm. Such measurements will accelerate understanding of localized electromagnetic modes. The exponential profile observed sheds new light on the much-debated mechanism of extraordinary field confinement in a two-dimensional disordered system where Anderson-localized modes[4,15] could emerge. Although signatures of the Anderson-localized mode have been reported in two-dimensional disordered metallic systems[16], its hallmark, an exponential profile, had not been directly observed up until now. Additionally, other imaging modalities can be integrated to provide spectroscopy as well as fluorescence lifetime information on the molecules; this approach could be used to investigate the strong-coupling regime such as occurs with resonant nano-antennas[29,30]. In the strong-coupling regime, the distributed dipoles in the antenna could significantly affect the fluorescence of the molecules, and the strength of the coupling cannot be directly measured from the intensity of the fluorescence signals. A super-resolution measurement of the spatial distribution of the molecules' fluorescence lifetime will help visualization and understanding of the coupling. Furthermore, with the development of brighter fluorophores, better photo-bleaching suppression methods, and more efficient three-dimensional super-resolution techniques, three-dimensional imaging will also be realized.

METHODS SUMMARY

Details of the experiment can be found in Methods. There we describe the fabrication of the aluminium film on a quartz slide, the self-assembly of silver nanoparticle clusters on a glass cover slide, the prism-TIRF experiment for the observation of the

hotspots on the aluminium film, the objective-TIRF experiment for the observation of the hotspots in silver nanoparticle clusters, the single-molecule localization method used to determine the adsorption centre and the fluorescence intensity of each single-molecule events, and the Gaussian kernel method for image rendering. More discussion on the single-molecule localization and the imaging rendering methods can be found in the Supplementary Information.

Full Methods and any associated references are available in the online version of the paper at www.nature.com/nature.

1. Kneipp, K. *et al.* Single molecule detection using surface-enhanced Raman scattering (SERS). *Phys. Rev. Lett.* **78,** 1667–1670 (1997).
2. Nie, S. & Emory, S. R. Probing single molecules and single nanoparticles by surface-enhanced Raman scattering. *Science* **275,** 1102–1106 (1997).
3. Shalaev, V. M. & Stockman, M. I. Fractals: optical susceptibility and giant Raman scattering. *Z. Phys. D* **10,** 71–79 (1988).
4. Stockman, M. I., Faleev, S. V. & Bergman, D. J. Localization versus delocalization of surface plasmons in nanosystems: can one state have both characteristics? *Phys. Rev. Lett.* **87,** 167401 (2001).
5. Betzig, E. & Trautman, J. K. Near-field optics: microscopy, spectroscopy, and surface modification beyond the diffraction limit. *Science* **257,** 189–195 (1992).
6. Nelayah, J. *et al.* Mapping surface plasmons on a single metallic nanoparticle. *Nature Phys.* **3,** 348–353 (2007).
7. Vesseur, E. J. R., de Waele, R., Kuttge, M. & Polman, A. Direct observation of plasmonic modes in Au nanowires using high-resolution cathodoluminescence spectroscopy. *Nano Lett.* **7,** 2843–2846 (2007).
8. Kubo, A., Jung, Y. S., Kim, H. K. & Petek, H. Femtosecond microscopy of localized and propagating surface plasmons in silver gratings. *J. Phys. At. Mol. Opt. Phys.* **40,** S259–S272 (2007).
9. Jeanmaire, D. L. & Van Duyne, R. P. Surface Raman spectroelectrochemistry: Part I. Heterocyclic, aromatic, and aliphatic amines adsorbed on the anodized silver electrode. *J. Electroanal. Chem.* **84,** 1–20 (1977).
10. Albrecht, M. G. & Creighton, J. A. Anomalously intense Raman spectra of pyridine at a silver electrode. *J. Am. Chem. Soc.* **99,** 5215–5217 (1977).
11. Fleischmann, M., Hendra, P. J. & McQuillan, A. J. Raman spectra of pyridine adsorbed at a silver electrode. *Chem. Phys. Lett.* **26,** 163–166 (1974).
12. Creighton, J. A., Blatchford, C. G. & Albrecht, M. G. Plasma resonance enhancement of Raman scattering by pyridine adsorbed on silver or gold sol particles of size comparable to the excitation wavelength. *J. Chem. Soc. Faraday Trans. 2* **75,** 790–798 (1979).
13. Moskovits, M. Surface roughness and the enhanced intensity of Raman scattering by molecules adsorbed on metals. *J. Chem. Phys.* **69,** 4159–4161 (1978).
14. Gersten, J. & Nitzan, A. Electromagnetic theory of enhanced Raman scattering by molecules adsorbed on rough surfaces. *J. Chem. Phys.* **73,** 3023–3037 (1980).
15. Sarychev, A. K., Shubin, V. A. & Shalaev, V. M. Anderson localization of surface plasmons and nonlinear optics of metal-dielectric composites. *Phys. Rev. B* **60,** 16389–16408 (1999).
16. Seal, K. *et al.* Coexistence of localized and delocalized surface plasmon modes in percolating metal films. *Phys. Rev. Lett.* **97,** 206103 (2006).
17. Hutchison, J. A. *et al.* Subdiffraction limited, remote excitation of surface enhanced Raman scattering. *Nano Lett.* **9,** 995–1001 (2009).
18. Betzig, E. *et al.* Imaging intracellular fluorescent proteins at nanometer resolution. *Science* **313,** 1642–1645 (2006).
19. Rust, M. J., Bates, M. & Zhuang, X. W. Sub-diffraction-limit imaging by stochastic optical reconstruction microscopy (STORM). *Nature Methods* **3,** 793–796 (2006).
20. Sharonov, A. & Hochstrasser, R. M. Wide-field subdiffraction imaging by accumulated binding of diffusing probes. *Proc. Natl Acad. Sci. USA* **103,** 18911–18916 (2006).
21. Wu, D., Liu, Z., Sun, C. & Zhang, X. Super-resolution imaging by random adsorbed molecule probes. *Nano Lett.* **8,** 1159–1162 (2008).
22. Hell, S. W. in *Single Molecule Spectroscopy in Chemistry, Physics and Biology* (eds Gräslund, A., Rigler, R. & Widengren, J.) 365–398 (Springer Series in Chemical Physics, Springer, 2009).
23. Roeffaers, M. *et al.* Super-resolution reactivity mapping of nanostructured catalyst particles. *Angew. Chem.* **121,** 9449–9453 (2009).
24. Mortensen, K. I., Churchman, L. S., Spudich, J. A. & Flyvbjerg, H. Optimized localization analysis for single-molecule tracking and super-resolution microscopy. *Nature Methods* **7,** 377–381 (2010).
25. Chang, C. C. *et al.* Aluminum oxidation in water. *J. Electrochem. Soc.* **125,** 787–792 (1978).
26. Wokaun, A., Lutz, H. P., King, A. P., Wild, U. P. & Ernst, R. R. Energy transfer in surface enhanced luminescence. *J. Chem. Phys.* **79,** 509–514 (1983).
27. Chance, R. R., Prock, A. & Silbey, R. Comments on the classical theory of energy transfer. *J. Chem. Phys.* **62,** 2245–2253 (1975).
28. Anger, P., Bharadwaj, P. & Novotny, L. Enhancement and quenching of single-molecule fluorescence. *Phys. Rev. Lett.* **96,** 113002 (2006).
29. Taminiau, T. H., Stefani, F. D., Segerink, F. B. & van Hulst, N. F. Optical antennas direct single-molecule emission. *Nature Photon.* **2,** 234–237 (2008).
30. Kinkhabwala, A. *et al.* Large single-molecule fluorescence enhancements produced by a bowtie nanoantenna. *Nature Photon.* **3,** 654–657 (2009).

Author Contributions H.C., A.L., X.Y. and X.Z. designed the experiments; H.C., A.L., C.G. and M.L. conducted experiments; C.L. and Y.L. conducted computer simulations and theoretical analysis; H.C., A.L., X.Y. and X.Z. wrote the paper.

METHODS

Observations of hotspots on aluminium films. A quartz slide (3 inch × 1 inch, Ted Pella or SPI) is thoroughly cleaned according to a protocol developed at Radio Corporation of America (RCA protocol), before deposition. First, the slide is soaked in a bath of a base solution (distilled water, hydrogen peroxide and ammonium hydroxide at a ratio of 4:1:1) for 15 min; it is then transferred to an acid bath (distilled water, hydrogen peroxide and hydrogen chloride at a ratio of 6:1:1) for another 15 min, followed by 15 min of sonication in filtered distilled water (Milipore). The slide is then blow-dried with pure nitrogen gas and placed immediately inside an electron-beam evaporation chamber (Torr International). After the vacuum is pumped down to a minimum of 10^{-6} torr, deposition is started at a deposition rate of $0.1\,nm\,s^{-1}$. A crystal detector monitors the thickness of the film in real time. The deposition stops once the thickness reaches 15 nm.

A flow chamber is made by sandwiching an aluminium coated quartz slide and a clean glass cover slip using double-sided tape. The glass cover slips (no. 0, Ted Pella) are cleaned following the same procedure used for cleaning the quartz slide and stored in a clean jar filled with filtered distilled water before use. The chamber is placed on a home-built prism type total internal reflection (TIRF) microscope. A 200-mW 532-nm laser (Lambda Service) is used as the excitation light. The intensity is adjusted by neutral density filters to about 7 mW measured immediately before the prism. A 1-nm laser line band pass filter (Edmunds Optics), centred at 532 nm, is used to clean the excitation light that then impinges on a quartz Pellin-Broca prism (Thorlabs) and excites an evanescent wave on the surface of the sample. A 60×, NA 1.25 objective lens (Zeiss) is used to collect the light, and an electron multiplying charge coupled device (EMCCD Cascade 512, Photometric) is used to record fluorescent images. A 532-nm long pass filter (Semrock) and a band pass filter whose centre wavelength and bandwidth are 582 nm and 80 nm, respectively (582/80m from Chroma Technology), are placed after the objective lens. A 4× magnifier (Nikon) is placed right in front of the EMCCD in order to make the pixel size 72 nm. The camera's exposure time is 80 ms.

Filtered distilled water (Milipore) is first poured into the chamber. 10 nM Chromeo 542 dye (Active Motif) in filtered distilled water (Milipore) is then flowed into the chamber. Other dyes, including Cy3 (GE Healthcare), and Alexa-555 (Life technology) yield similar results. Immediately after the dye is flowed in, the fluorescence background increases significantly. Blinking at some spots was immediately observed and recorded. To avoid errors caused by the slow drifting of the objective lens, the total recording time is limited to a few minutes. To compare the enhancement factor, a similar experiment is performed in a quartz flow chamber without aluminium film coating, with a dye concentration of ~1 nM.

Observations of hotspots on silver nanoparticle clusters. Glass cover slips (no. 1.5, Fisher Scientific) are cleaned following the same procedure used for cleaning the quartz slide. The cleaned cover glass is stored in a clean jar filled with filtered distilled water before use. A drop of 0.1 ml concentrated solution of 40 nm silver colloids (Ted Pella) is coated on a cleaned cover glass. As the water evaporates, a layer of nanoparticle clusters formed on the surface. A home-built objective type TIRF with a Nikon TIRF objective (NA 1.49, 100×) is used. The excitation beam from a 40-mW 644-nm laser (Coherent, Cube) is reflected by a dichroic mirror with transition edge at 650 nm (650DCLP Chroma) into the objective lens. The power at the objective lens is measured to be ~4 mW. An emission filter (710/130m Chroma), whose centre and bandwidth are 710 nm and 130 nm respectively, is used before an EMCCD camera (Cascade 512, Princeton Instruments). To reduce the pixel size, a 4× magnifier (Nikon) is placed right in front of the EMCCD. The final pixel size corresponds to 48 nm per pixel. 10 nM Chromeo 642 dye (Active Motif) solution is used for the single molecule super-resolution imaging. The exposure time of the camera is 20 ms.

Single-molecule localization. This is performed by using a maximum likelihood estimation method[24]. Briefly, the log likelihood function

$$\sum_i \left(-E_i + n_i \log E_i - \log(n_i!) \right)$$

where n_i is the observed number of photons at pixel i, and E_i is the expected number of photons calculated from the fitting parameters, is minimized. The accuracy of the estimation, determined from the variance, is:

$$\mathrm{Var}(x) = 2\frac{\sigma_\alpha^2}{N}\left(1 + \int_0^1 dt\, \frac{\log(t)}{1+t/\tau} \right)$$

Since each pixel of a camera has a finite size of a, the width of the Gaussian PSF has to be corrected as $\sigma_a^2 = \sigma^2 + a^2/12$. N is the total number of photons observed from the raw image. The integration in the bracket accounts for the shot noise from the background photons as $\tau = 2\pi\sigma_a^2 b^2/Na^2$, where b is the average background photon count[24]. The factor of 2 corrects the gain noise from an EMCCD camera.

We performed the single molecule localization in two steps: a least squares fitting of the raw image to a 2D Gaussian function is first used to obtain the initial parameters, and then the parameters are fed into the maximum likelihood estimation method to extract the centroid position x and y, and the amplitude, which are then used to generate the 3D scatter plot shown in Fig. 1.

Gaussian kernel image rendering. The collected single molecule events distribute in a random and sparse manner in space. As it is difficult to apply a fixed mesh directly for image rendering, we use a Gaussian Kernel rendering procedure.

Each image spot is analysed by a maximum likelihood estimation method[24] to extract the centroid position x, y and the intensity I. We then assign each single molecule event, represented by a colour sphere in the 3D scatter plot, to a Gaussian function, with the peak position as x and y, and the width as σ, determined from the accuracy of the single molecule localization by equation (1). The Gaussian function thus represents the probability of finding the true location of the single molecule event in space.

$$I(\mathbf{x}) = \sum I_i \exp\left(-(\mathbf{x}-\mathbf{x}_i)^2/2\sigma^2 \right) \Big/ \sum \exp\left(-(\mathbf{x}-\mathbf{x}_i)^2/2\sigma^2 \right)$$

Multiplying each Gaussian function with the intensity I_i from the fitting, summing them up, and normalizing the sum by the mean number of events, provides a smooth 3D image of the enhancement profile.